npj | heritage science

Article

https://doi.org/10.1038/s40494-026-02318-9

Determination of interfacial heat transfer coefficient between bronze and loess-based molds in Bronze Age China

Check for updates

Huan Yang[1] ✉, Minghui Fang[2], Tonia Eckfeld[3], Jiangning Song[4] & Junchang Yang[1]

In early Chinese civilization loess-based clay mold technology was instrumental to both the mass production of ritual bronzes and the development of metallurgical traditions. A comprehensive understanding of ancient Chinese bronze casting technology requires quantitative investigations into the functional performance of clay molds. Building on measurements of the thermophysical parameters of clay molds unearthed at a Western Zhou-period bronze foundry, this study establishes a one-dimensional unsteady heat transfer model. By combining this model with experiments to monitor the temperature of flat-plate molds, and Beck's nonlinear estimation with supporting data validation, the interfacial heat transfer coefficient between bronze alloy and clay molds during the casting process is derived for the first time. This study provides accurate parameters for conducting numerical simulations on bronze casting processes and functionality by focusing on the quantitative analysis of casting performance, and establishes a methodological framework to address pivotal archaeometallurgical questions for future studies.

China's Bronze Age was characterized by the use of bronze vessels for ritual ancestral and divine worship. Distinct from the lost-wax casting methods prevalent in other civilizations at that time, Shang-Zhou artisans employed piece-mold casting techniques using earthen materials to create clay molds with precise mold cavities, and produce near-perfect bronze castings.

Gettens et al. have demonstrated that the locations of Chinese bronze casting sites strongly correlated to loess distribution[1]. Quantitative research on the casting performance of clay molds is necessary to identify the essential characteristics of ancient Chinese metalworking. Furthermore, this sheds light on the performance of clay molds during the casting process and reveals potential differences in the casting functionality of clay molds belonging to different periods and areas. Major bronze-casting sites from the Shang-Zhou period identified to date, including the Anyang foundry (late Shang Dynasty, loess thickness: 100–50 m), the Zhouyuan foundry (Western Zhou period, loess thickness: 200–100 m), and the Houma foundry (Spring and Autumn and Warring States periods, loess thickness: 100–50 m), are predominantly concentrated within the Loess Plateau region of the Yellow River Basin (Fig. 1) (both the loess thickness distribution data and Fig. 1 are sourced from Li et al. [2]). Native loess deposits across vast geographical regions, proved universally suitable for bronze casting after being proportioned and fired by artisans.

Clay mold research has been ongoing since they were first discovery in 1932[3] at the Yin Ruins (Anyang, Henan province). Significant studies on the casting performance of excavated clay molds by Lian Haiping[4], Tan Derui, and others, have obtained data on their density, granularity, thermal expansion, and other properties. These studies also identified factors influencing metal filling capacity, including mold heat storage coefficient (b_2), density (ρ_2), specific heat capacity (C_2), thermal conductivity (λ_2), mold gas release and permeability, and contact angle[5,6]. Studies conducted by Liu et al. [7] and Tian[8] examined other properties of clay molds, such as their particle size[9,10], permeability, water absorption rate, gas release, mechanical properties, and thermal shock resistance[6–11]. While previous studies expanded understanding of the performance parameters of clay molds, more recent studies focused predominantly on the material properties of molds. These studies have not, however, revealed the core functional mechanisms of clay molds in the casting process, and have not performed quantitative characterizations of their thermal behavior.

Modern casting theory posits that molds must serve two distinct functions: cavity formation and thermal regulation[11]. In bronze casting, cavity configuration involves the geometric control of wall thickness, patterns, and gating system design, while thermal regulation necessitates clay mold materials to exhibit appropriate thermophysical properties and critical boundary conditions, such as the pouring temperature, the mold

[1]Institute of Culture and Heritage, Northwestern Polytechnical University, Xi'an, China. [2]School of Materials Science and Engineering, Northwestern Polytechnical University, Xi'an, China. [3]School of Historical and Philosophical Studies, The University of Melbourne, Melbourne, VIC, Australia. [4]Institute of Archaeology of Chinese Academy of Social Sciences, Beijing, China. ✉e-mail: yanghuan2019@nwpu.edu.cn

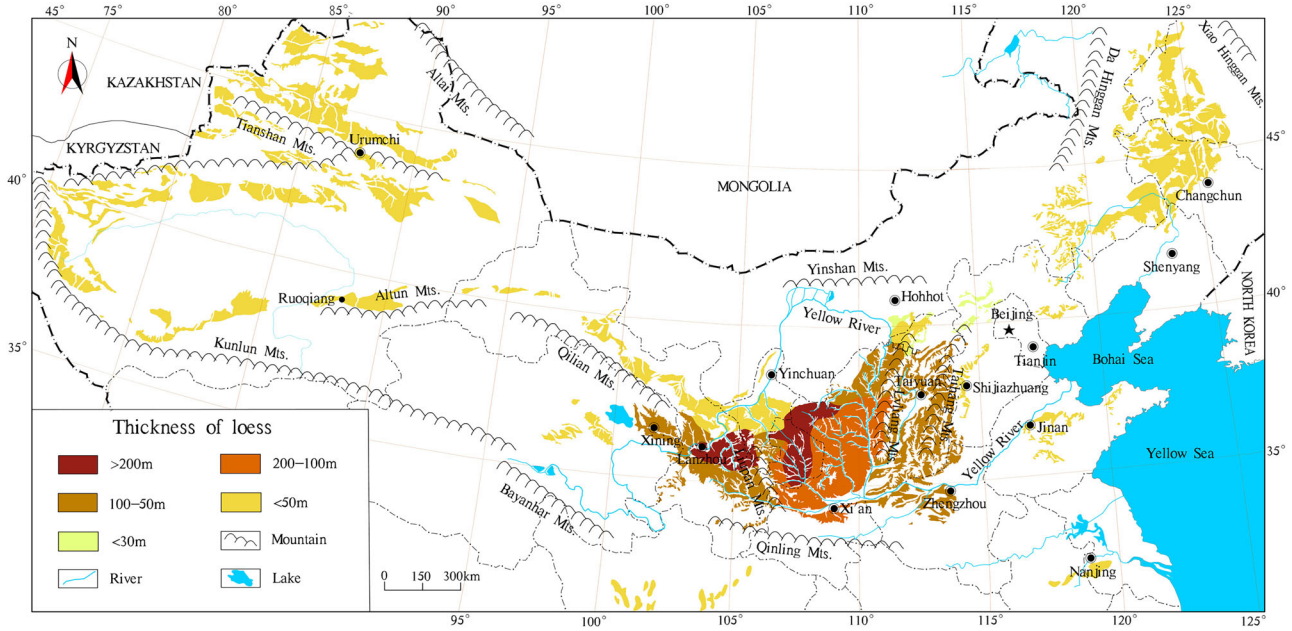

Fig. 1 | Map of Loess Resources Distribution in China. Reproduced from Li et al.[2], with permission from Elsevier.

temperature, and, particularly, the interfacial heat transfer coefficient (IHTC). Interfacial heat transfer behavior critically determines the casting solidification process and final material properties. In the modern foundry industry, experimentally measured IHTC values are employed as boundary conditions in numerical simulations to quantitatively evaluate the heat transfer effects across mold materials, enabling optimal mold selection. IHTC is a comprehensive measure of the interfacial heat exchange behavior between molds and castings[12–14].

IHTC can comprehensively characterize the performance of the clay mold during the entire pouring and solidification process, with additional parameters such as the mold's surface texture, geometric configuration, and dimensional specifications. Quantitative analysis of the IHTC between different clay molds, and molten/solid bronze, can advance the study of ancient bronze technology from qualitative description to quantitative analysis. IHTC enables researchers to systematically simulate the effects of different mold materials on the performance of bronze artefacts, and thereby precisely decipher the scientific principles underlying China's ancient loess-based piece-mold casting technology. The casting simulation software database does not, however, include the parameters for ancient clay molds. Determining such parameters is, therefore, a crucial further step[15–17].

In order to address the computational challenges of determining the IHTC of ancient casting materials, this study analyzed collected clay mold samples from the Western Zhou period Zhouyuan Foundry site in Baoji, Shaanxi Province. Following measurement and calculation of the density, thermal conductivity, and specific heat capacity of these clay molds, new temperature-monitoring clay molds were fabricated using local loess. Utilizing the preliminary data obtained, an inverse calculation method combined with data validation was implemented to accurately derive the IHTC values for the clay molds and castings. These results are important as they provide the interfacial heat transfer parameters for ancient materials for the first time.

Methods

Currently, there are three commonly used methods to determine IHTC: the interface air gap method, the interface temperature difference method, and the inverse calculation method[14,18]. Since directly measuring the gap thickness and interfacial temperatures using displacement or temperature sensors is challenging, while the inverse calculation method requires only temperature fields at specific nodes within the casting and mold, it is easier to implement and has therefore become the most widely adopted and effective approach for obtainining IHTC[19–21]. The specific steps of the inverse calculation method include: conducting a heat transfer analysis of the casting process of ancient Chinese bronze vessels using the finite difference method (FDM), establishing a one-dimensional unsteady heat transfer model, and designing an experimental set up based on a flat-plate mold to measure the temperature of the clay mold and the alloy. After combining the aforementioned data with the thermophysical properties of clay molds, Beck's nonlinear estimation method is employed to determine the interface temperature (T_{mold}), interfacial heat flux (q), and the clay mold IHTC (h).

Experimental design

This study used a flat-plate model (Fig. 2) with the thickness and side length of the casting set to 3 and 150 mm, respectively. The flat-plate model was composed of two rectangular clay mold pieces, each with a thickness of 32 mm (Fig. 2c). One mold piece had a flat inner wall, while the other included a gating system, a cavity, and a riser on its inner surface. The sprue and riser were positioned in the upper part of the mold (Fig. 2a).

Five sets of K-type sheathed thermocouples were employed to measure the temperature of the mold in specific locations. Considering the actual working conditions, the thermocouple used for measuring the alloy temperature had dimensions of $\varphi 2 \times 200 \times 2000$ mm, while those used for measuring the temperature at the clay mold nodes had dimensions of $\varphi 4 \times 50 \times 2000$ mm, where φ denotes the diameter of the thermocouple. The thermocouple for measuring the alloy temperature was positioned in the riser, whereas the thermocouples for measuring the clay mold temperature were located at distances of 6, 14, 22, and 30 mm from the interface between the casting and the mold (Fig. 2b).

It should be noted that, while the physical clay mold and the 3D model have slightly different dimensions in central thickness and the gating and riser system, their temperature measurement function remains consistent, and these geometric discrepancies are not considered to introduce experimental error. The gating and riser ensure successful filling of the casting, and, providing they are reasonably configured, do not affect the temperature measurement results. For this reason, no specific requirements were imposed on their location or dimensions in the 3D model. To prevent cracking during the mold fabrication process, the central portion of the physical clay mold was intentionally thickened to ~45 mm in order to obtain a slightly curved surface. During drilling, a vernier caliper was used to aid positioning so that the distance between each thermocouple placement point and the casting–mold interface

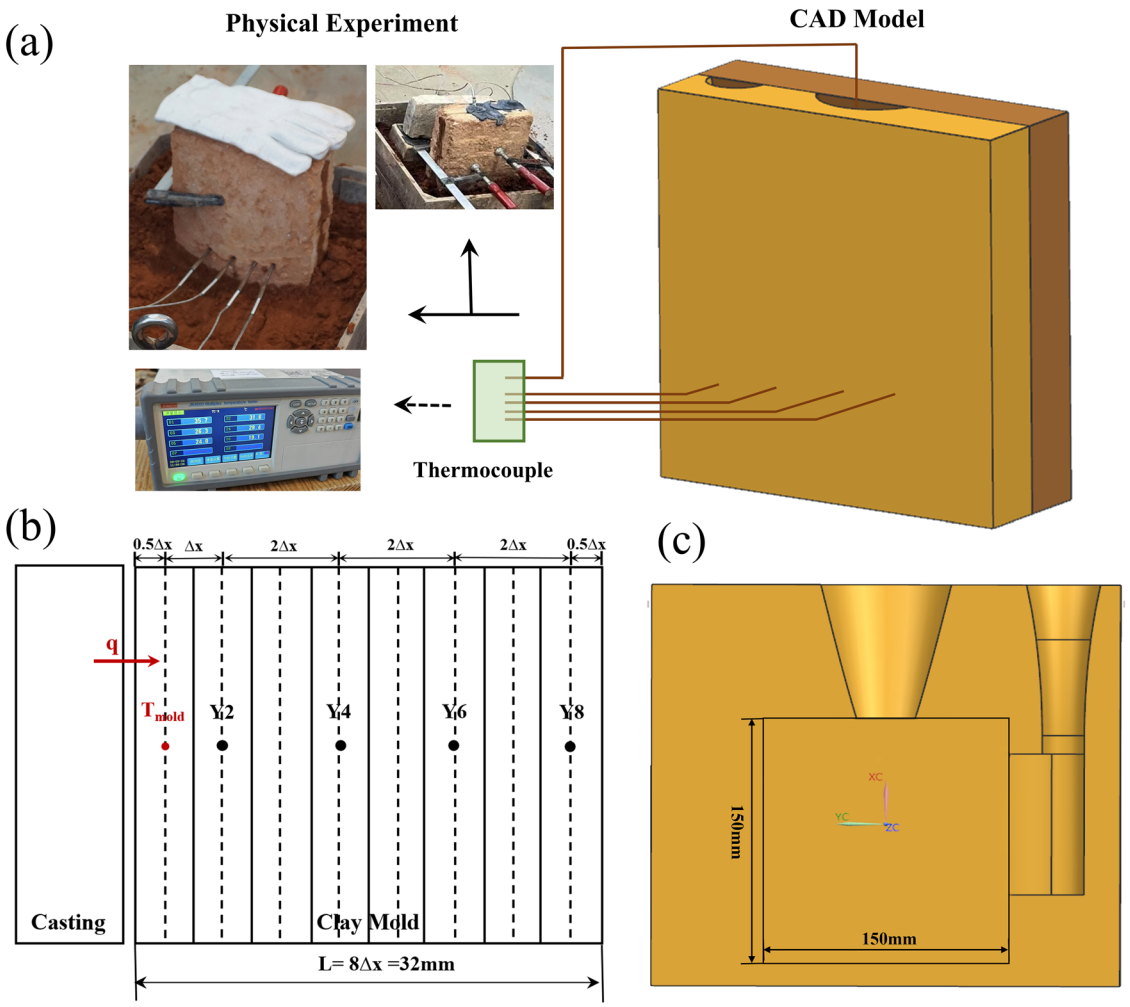

Fig. 2 | Schematic of the experimental device used to measure the temperature (alloy composition: $Cu_{90}Sn_{10}$, pouring temperature: 1100 °C). a Photograph and schematic of the experimental setup. **b** Locations of the installed thermocouples. **c** Internal structure and dimensions of the casting for temperature measurements.

Table 1 | Thermophysical parameters of clay mold samples excavated from the Zhouyuan Zhuangli Foundry

Sample no.	Density(AVE) Kg/m^3	Specific heat capacity J/ (Kg·K)	Thermal conductivity W/(m·K)
H6-2 (measured)	2167	785.4–1339.7	0.74–0.95
H6-2 (simplified)	2167	1000	1

matched the design specification. This ensured that the temperature measurement results were not affected.

The alloy material used in this study was $Cu_{90}Sn_{10}$ bronze, the pouring temperature was maintained at 1100 °C, and the pouring time was 4 s. The casting mold was crafted from local loess collected from the Zhouyuan Zhuangli Foundry, using traditional clay mold fabrication methods. The thermophysical parameters of the clay mold were obtained through experimental measurements of ancient mold samples unearthed at the Zhouyuan Zhuangli Foundry of Western Zhou dynasty. These parameters were subsequently simplified for use in later calculations (Table 1). The details of the experimental methods will be published in a separate article.

Correction of the measured temperature data

Since the calculated IHTC values are highly sensitive to temperature measurement errors, it is essential to conduct an error analysis and perform corresponding corrections for the temperature data. Considering factors such as the thermocouple dimensions and temperature measurement range, this study assumes that the measured alloy temperatures are error-free, and thus focuses only on correcting errors in the measured clay mold temperatures.

Due to the time required for the heat flux to propagate from the interface to the location of the thermocouple probe head, the penetration time t_p is defined as the time taken by the sensor to overcome a heat flux threshold, which was set to 1% of the interface temperature change. Based on the experimental data and analytical value, the Fourier number (F_o) was determined to be 0.075 according to Eq. (1)[22], where F_{o_p} is dimensionless penetration time, d is the distance from the surface to the embedded sensors (m), and α is the thermal diffusivity (m²/s). The t_p for each temperature measurement channel was calculated using this equation and then subtracted from the original temperature measurement data (Table 2). The resulting temperature (with t_p removed) was used as the measured temperature for subsequent calculations.

$$t_p = F_{o_p}\frac{d^2}{\alpha} = 0.075\frac{d^2}{\alpha}. \quad (1)$$

At the same time, thermocouples exhibit dynamic response characteristics. When the initial interface temperature changes rapidly, the heat

transfer from the protective sheath, through the filled MgO, to the ungrounded junction and wire introduces a delay, resulting in a difference between the measured and actual temperatures. This delay is called the time constant of thermocouples. The time constant of the sheathed thermocouple can be determined by formulating a differential equation based on the energy balance equation and the heat transfer between the sheath and the thermocouple, combined with experiments[23]. In this study, Jaremkiewicz's temperature correction method for transient fluid temperature measurements was employed. The temperature measurement system was modeled as a first-order inertial device, with the air gap and radiation heat transfer between the sheath and the temperature sensor neglected. The evolution of the thermocouple-measured temperature T with time t was described using the following ordinary first-order differential equation[24]:

$$\tau \frac{\mathrm{d}T}{dt} + T = T_{act}, \tag{2}$$

where τ represents the first-order time constant, and T_{act} denotes the actual fluid temperature. The value of τ should be determined through a temperature response experiment. However, given the relative simplicity of the heat transfer model employed in this study, we referred to the approximate time constant measured by Jaremkiewicz for a 1.5 mm sheathed thermocouple at zero air velocity to better represent the actual conditions in the present work. Accordingly, the experimental time constant of sheathed thermocouples in different conditions was set to 30 s[24].

Establishment of the numerical heat transfer model

Based on the excavated bronzes and restoration experiments, the wall thickness of the flat-plate casting was set to 3 mm, and the clay mold thickness was set to 32 mm[25]. The Biot number (Bi) is defined as the ratio of thermal resistance within the casting to the interfacial thermal resistance between the casting and mold. According to Eq. (3), the Biot number (Bi) approaches zero[26], indicating that before the bronze starts to solidify, the internal conduction resistance can be neglected, the temperature field within the molten alloy is uniform, and the heat flux q is basically the same at different locations. Consequently, the model is simplified to a one-dimensional unsteady heat transfer without internal heat sources. If the actual Biot number is not small but the model assumes a one-dimensional unsteady heat transfer, the internal temperature drop within the casting may be incorrectly attributed to the interface, leading to an overestimation of the interfacial thermal resistance and thus an underestimation of the IHTC during inverse identification.

$$Bi = \frac{\delta h}{\lambda} = \frac{0.0015 \times 500}{50} = 0.015 \to 0 \tag{3}$$

Where 2δ represents the wall thickness of the bronze, h denotes the IHTC between the casting and the mold (assumed to have a relatively large value)[27], and λ refers to the thermal conductivity of the bronze alloy liquid (assumed to have a rather small value).

For the above model, the FDM was employed to perform numerical simulations, which involves dividing the alloy melt and clay mold into numerous infinitesimally small cubic volumes. Unit 0 represents the bronze, units 1 and 8 are the boundary control units, and units 2–7 are the internal control units. The right boundary condition is defined as a first-type boundary condition, and the left boundary $\vec{q}$ represents the heat flux from the casting to the clay mold interface, which corresponds to a second-type boundary condition.

The unit nodes are positioned at the center of the control units, a with a unit length of 4 mm. This transformation simplifies the irregular shape of the bronze model into regular cubic elements, facilitating the computational modeling process. A discrete model is constructed by focusing on the interface between the casting and the clay mold, along with the adjacent regions (Fig. 3). The interface between the casting and the clay mold is consequently treated as a homogenous plane with a finite thickness, where heat transfer occurs exclusively in the x-direction, while the temperature distribution is assumed to be uniform and extends infinitely in the y- and z-directions.

According to the law of energy conservation, the increase in internal energy within a control unit is equal to the total thermal energy entering the unit. This yields the general form of the differential equation for unsteady-state heat conduction:

$$\rho c \frac{\partial T}{\partial t} = \frac{\partial}{\partial x}(\lambda \frac{\partial T}{\partial x}) + \frac{\partial}{\partial y}(\lambda \frac{\partial T}{\partial y}) + \frac{\partial}{\partial z}(\lambda \frac{\partial T}{\partial z}) \tag{4}$$

Where c is the specific heat capacity ($\mathrm{J}/(\mathrm{kg} \cdot \mathrm{K})$), ρ is the density ($\mathrm{kg/m^3}$). According to Fourier's law of heat conduction, the heat flux in the x-direction can be expressed as:

$$\vec{q} = -\lambda \cdot \mathrm{grad}T = -\lambda \cdot \frac{\partial T}{\partial n} \cdot \vec{n} \tag{5}$$

Where $\vec{q}$ is the heat flux vector, $\vec{n}$ denotes the unit vector on the normal of the isothermal surface, which points to the side. Where the temperature is higher, $\partial T/\partial n$ represents the derivative of the temperature in the direction of the normal vector $\vec{n}$. The increase in internal energy at any time interval (Q) of the control unit ($\Delta x \Delta y \Delta z$) is given by:

$$Q = cmdT = \rho c dT \Delta x \Delta y \Delta z \tag{6}$$

Table 2 | Calculated penetration time t_p for different thermocouple locations

Thermocouple location	Y2	Y4	Y6	Y8
t_p (s)	6	32	79	147

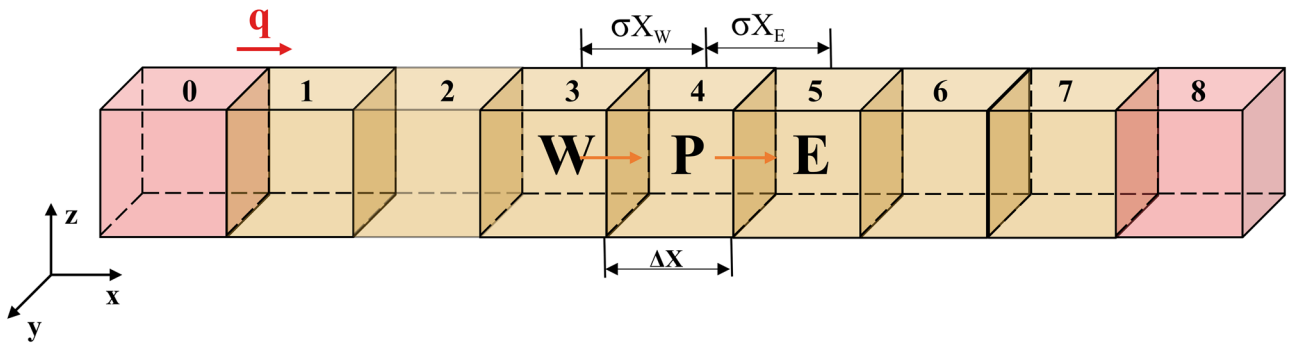

Fig. 3 | One-dimensional heat transfer model of clay mold.

where m is mass. Equations (4)–(6) can be combined as follows:

$$\rho c dT\Delta x = \lambda\frac{\partial T}{\partial x}\Delta t - \lambda\frac{\partial T}{\partial x}\Delta t. \tag{7}$$

Equation (7) was discretized using the time implicit scheme, which yielded a system of linear algebraic equations. To solve this system, it is necessary to know the temperature of all units at the previous time step, the boundary temperature at the current time step, and the interfacial heat flux q. The temperature at the previous time step can be determined through iteration after assigning the initial temperature, while the boundary temperature was obtained experimentally. Consequently, solving the entire equation system for the initial temperature field of the flat plate requires only the interfacial heat flux q. For subsequent time steps, q can be computed through iterative solving.

Inverse calculation method for the IHTC

This study applies Beck's nonlinear estimation method to inversely compute the IHTC between the casting and the mold. In this method, the interfacial heat flux q is typically discretized into N constant heat flux values q with a time interval of Δt. When solving for the heat flux at time t, it is assumed that the heat flux values remain constant within R time steps after t (Eq. (8)). This approach enables the determination of the temperature field at R future time steps[28]. By adopting this method, the process of solving the equations is significantly expedited, and storage space requirements are reduced.

$$q_t = q_{t+1} = q_{t+2} = \cdots\cdots = q_{t+R-1} \tag{8}$$

The objective function $F(q_t)$ used in in the iterative optimization problem is defined as follows:

$$F(q_t) = \sum_{j=1}^{J}\sum_{i=0}^{R-1}\left(T_{j,t+i}^{m} - T_{j,t+i}^{c}\right)^2 \tag{9}$$

Where $T_{j,t+i}^{m}$ and $T_{j,t+i}^{c}$ represent the measured and calculated temperatures at the thermocouple node j and at the time step $t+i$, respectively. q_t is the heat flux at time t, and J and R denote the total number of temperature measurement points and the total number of future time steps, respectively[17]. To achieve convergence, it is necessary to calculate the sensitivity coefficients Φ and Δq_t, which are defined by the two following equations, respectively:

$$\Phi_{j,t+i}^{t} = \frac{\partial T_{j,t+i}^{c}(q_t)}{\partial q_t}, \tag{10}$$

$$\Delta q_t = \frac{\Sigma_{j=1}^{J}\Sigma_{i=0}^{R-1}\left(T_{j,t+i}^{m} - T_{j,t+i}^{c}\right)\Phi_{j,t+i}^{t}}{\Sigma_{j=1}^{J}\Sigma_{i=0}^{R-1}\left(\Phi_{j,t+i}^{t}\right)^2}. \tag{11}$$

Once the heat flux has been updated, it can be checked whether the computation has converged. The convergence condition is defined by the following inequality:

$$\frac{\Delta q_t}{q_t} < \varepsilon. \tag{12}$$

Once the convergence condition is satisfied, the heat flux q and the temperature field are derived, and the following iteration cycle starts. Finally, the IHTC is calculated using Eq. (13) below. The flowchart of this iterative calculation method is presented in Fig. 4.

$$h = \frac{q_t}{T_{casting} - T_{mold}} \tag{13}$$

Where $T_{casting}$ is the alloy temperature, and T_{mold} is the interfacial temperature between the clay mold and the casting.

Considering that the Biot number approaches zero, the temperature field of the casting can be regarded as uniform. The alloy temperature, $T_{casting}$, in Eq. (13) can be directly measured using a thermocouple. However, directly measuring the clay mold interface temperature, T_{mold}, with a thermocouple presents significant challenges, including the difficulty of drilling and the risk of damaging the clay mold due to thermal expansion during pouring. To overcome these issues, this study employed a numerical calculation method to estimate the clay mold interface temperature. A virtual control unit was established at the casting-mold interface, with the interfacial heat flux serving as the boundary condition. This boundary condition was then incorporated into the heat transfer equation to calculate the clay mold interface temperature, T_{mold}.

Results

Temperature field measurements and correction results

The experimental temperature values are shown in Fig. 5. The four temperature curves in black, which represent the clay mold nodes, should be referred to the left y-axis, while the temperature curve in red, which illustrates the casting during the whole pouring and solidification process, should be referred to the right y-axis. At ~19 s, the temperature of the red curve drops to 989 °C, marking the beginning of the solidification process; at around 125 s, the temperature further decreases to 676 °C, indicating the end of the solidification process.

During the initial stage of solidification, the temperature of the clay mold nodes does not exhibit a significant rise, and the corresponding temperature curves show minimal variation (Fig. 5). This is attributed to the penetration time of the temperature measurement equipment and the dynamic response characteristics of thermocouples. As the temperature changes over time and stabilizes, the temperature difference between the various nodes increases, particularly for units closer to the interface. However, the overall temperature of the mold nodes remains below 200 °C, indicating an extremely slow temperature rise and minimal heat transfer. This behavior can be explained by considering the material properties of the clay mold. Its high specific heat capacity enables it to absorb more heat without exhibiting a significant temperature increase, while its low thermal conductivity reduces the heat transfer between units.

Regarding the corrected temperature curves (Fig. 6), the four black curves represent the actual temperatures measured by the thermocouples at each node, while the four corrected temperature curves (which were obtained using the first-order correction model mentioned in Section "Correction of the measured temperature data") are shown in different colors. The smoothed corrected temperature curves, obtained using the Savitzky–Golay filter, were used for the subsequent inverse calculation and are represented by dotted lines of the same color.

Overall, the correction primarily affects the low-temperature region of the curves, where the discrepancy between the actual and corrected temperature values is caused by the equipment response and thermocouple delay in the initial temperature measurement stage (0–250 s). The trend of the corrected temperature curves is consistent with that of the original data, with differences becoming more noticeable closer to the interface. At the Y2 node, the difference between the corrected and original temperature values exceeds 20 °C, while at the Y4 node, it is within 10 °C. For the Y6 and Y8 nodes, the corrected temperature values are nearly identical to the measured temperature values, with a difference of ~1 °C.

This phenomenon indicates that the closer the measurement node is to the interface, where the heat flux changes dramatically, the greater are the influence of the heat flux penetration time and the thermocouple delay on the measured temperature data. Such influences have a greater impact on the accuracy of the obtained data during the initial temperature measurement stage (0–250 s). In the later stages ($t > 400$ s), the measured temperature data becomes stable and reliable, with errors due to the experimental setup no longer having a significant effect.

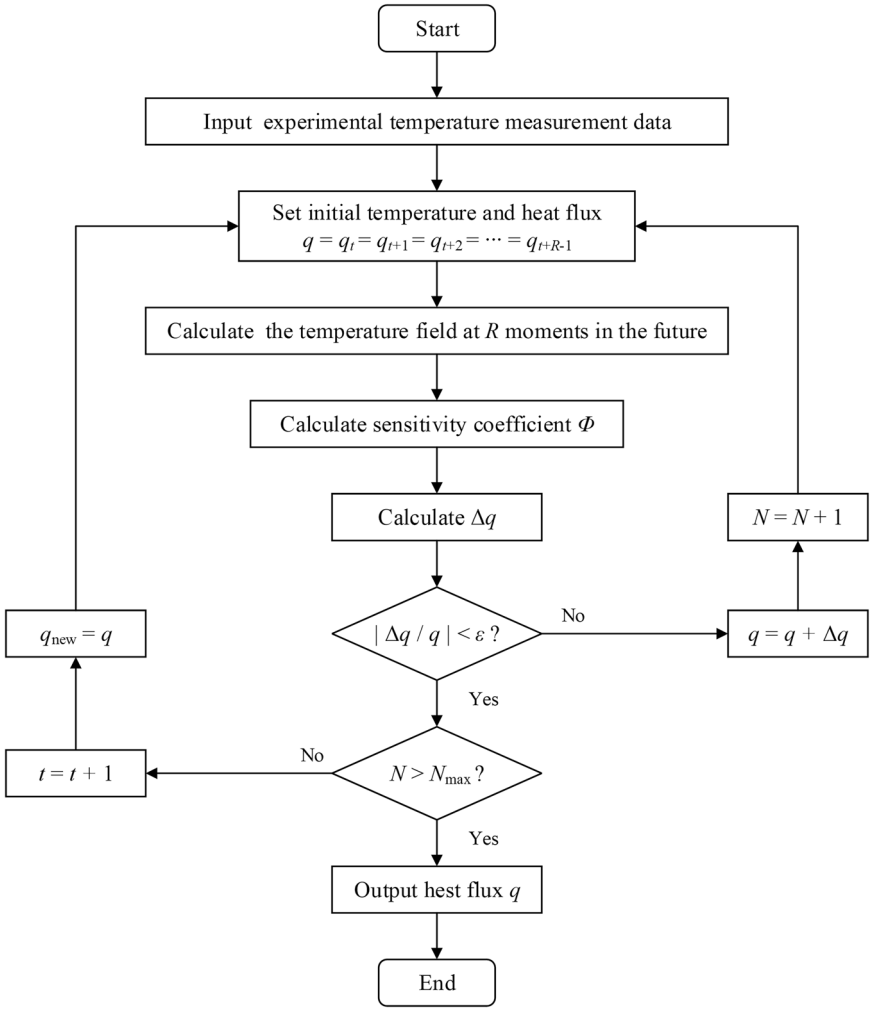

Fig. 4 | Schematic of the iterative calculation process for the IHTC.

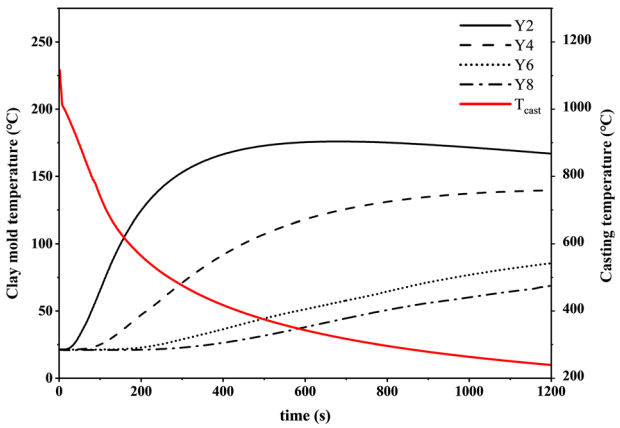

Fig. 5 | Experimental temperature data of the clay mold nodes and the casting. Black lines show the temperatures of the clay mold nodes. The red line shows the temperature of the casting.

Inverse calculation results for the IHTC

Figures 7 and 8 show the results of the inverse calculation, namely the interfacial temperature T_{mold} as a function of time and the interfacial heat flux and IHTC as a function of time, respectively.

Figure 7 illustrates the casting–clay mold interface temperature obtained from the inverse calculation alongside the corrected measurement data. The overall trend of the interface temperature closely resembles that of the temperature measured at other nodes, showing a rapid increase during the initial stage followed by a subsequent gradual decrease. Specifically, the interface temperature exhibits a sharp increase during the initial stage (0–50 s), reaching a maximum of ~215 °C, and a subsequent gradual decline.

The rates of the initial temperature rise and subsequent temperature drop at the interface are notably greaterthan the corresponding rates at other measurement nodes. At the end of the temperature measurement period, the interface temperature remains higher than that measured at the other nodes.

Figure 8a presents the results of the interfacial heat flux obtained from the inverse calculation. The black curve represents the values directly obtained from the inverse calculation software, while the blue curve is the heat flux curve derived from fitting the black curve. The resulting q values range from 0.0249×10^5 to 1.8625×10^5 W/m^2.

In typical sand-casting processes, the interfacial heat flux should exhibit a rapid change in the initial stage, peaking quickly before declining sharply. However, due to the response delay of the temperature measurement equipment and the thermocouples, the calculated heat flux in the initial stage tends to be lower than the actual value[29]. The original data obtained from the inverse calculation show a maximum, with the heat flux initially rising and then dropping during the initial stage (0–300 s). The maximum heat flux occurs at $t = 62$ s, although the peak is not prominent.

Additionally, the data fluctuates significantly within the temporal interval of 0–62 s. Owing to the delayed response of the thermocouple, the calculated heat flux during the initial stage (62–300 s) remains lower than the actual value, even after applying basic temperature correction. To

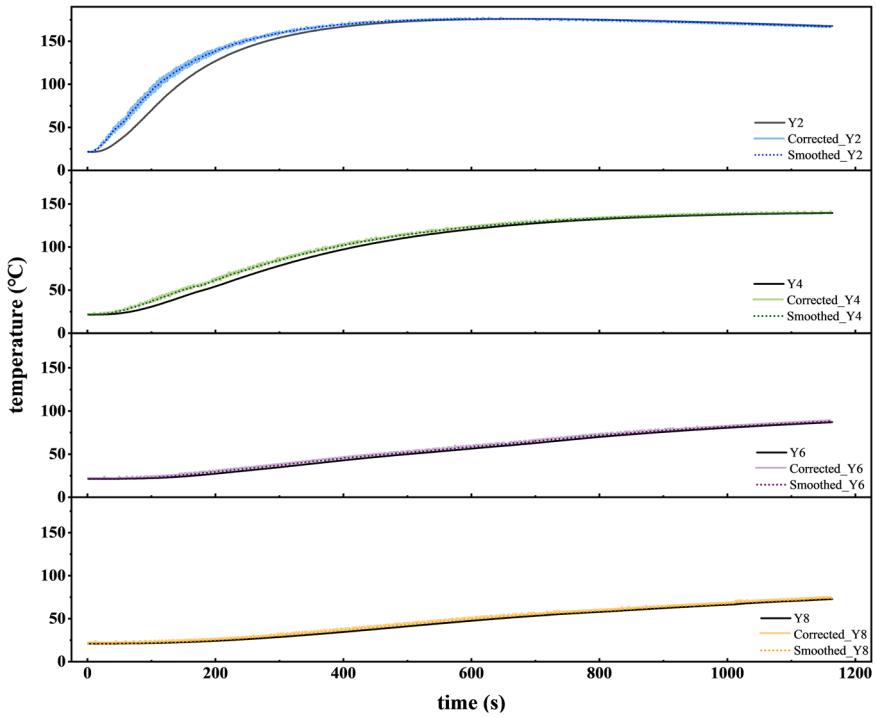

Fig. 6 | Original and corrected curves of the experimentally measured temperature fields. Black solid lines show the original temperatures; colored solid lines show the corrected temperatures; colored dotted lines show the smoothed temperatures.

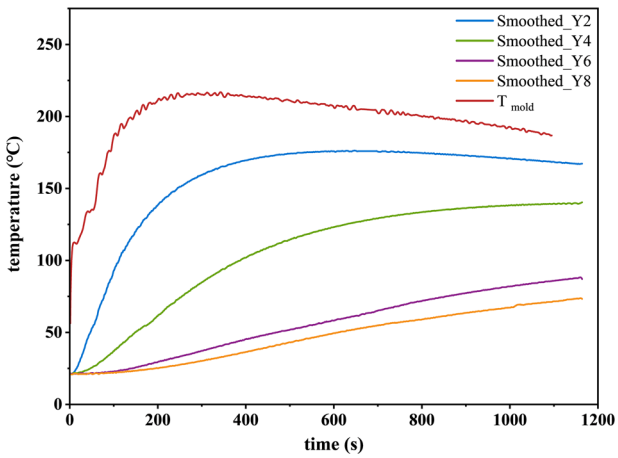

Fig. 7 | Smoothed Interface temperature derived from the inverse calculation method and measured temperatures of the clay mold.

overcome this issue, the data was fitted using a piecewise function. First, the unstable data in the range from 0 to 61 s was discarded, and the upper 50% of the data in the range from 62 to 300 s was selected for fitting a power function, in order to avoid a substantial deviation from the actual trend caused by the underestimated heat flux. The data beyond 300 s was considered reliable, consistent with the reliable nodes identified in the corrected temperature data. This portion of the data was fitted with the following polynomial function:

$$q(t) = \begin{cases} 1.86075 \times 10^5\, t^{-0.4} & , t < 62 \\ -8.1 \times 10^{-5} t^3 + 0.191 t^2 + 148.8 t + 4.37 & , t \geq 62 \end{cases} \quad (14)$$

It is evident that the interfacial heat flux q reaches an initial value of 1.8625×10^5 W/m^2 immediately after filling is completed and rapidly decreases to 0.3568×10^5 W/m^2 within 60 s (Fig. 8a). Thereafter, it gradually declines and eventually stabilizes at around 0.05×10^5 W/m^2. Combining these observations with Fig. 7, it becomes apparent that, in the initial stage, the high-temperature alloy liquid contains a substantial amount of thermal energy, which results in a significant amount of heat propagating to the interface.

As the temperature decreases and the solidification process starts, the interface becomes a solid–liquid–gas three-phase contact interface with the clay mold. Since the heat transfer rate of the solid phase is considerably lower than that of the liquid phase, the interfacial heat flux decreases rapidly. At ~125 s, the bronze cools to the solidus line, marking the end of the solidification process, and the interfacial heat flux drops to 0.2794×10^5 W/m^2. Beyond this point, the interfacial heat flux remains constant, indicating a stable state. This analysis highlights that the primary changes in the interfacial heat flux occur within the liquid–solid phase transition region.

The h–t curve (Fig. 8b) was obtained from Eq. (13), from which it can be seen that h is between 38.48 and 175.82 W/(m^2•K). The overall trend of the IHTC curve closely resembles that of the heat flux. The initial value, which is also the maximum value of the curve, is 175.82 W/(m^2•K). The heat flux then rapidly decreases to 50.86 W/(m^2•K) within 100 s and stabilizes around this value. The slight fluctuations observed in the figure are attributed to experimental and calculation errors.

The IHTC decreases rapidly in the liquid–solid phase transition region (0–100 s). This behavior is attributed to the shrinkage of bronze during cooling and solidification, which increases the air gap thickness between the casting and the mold. In the solid-phase region, the IHTC shows minimal change. This stability is explained by the negligible changes in the alloy volume and air gap size during this stage. Additionally, the temperature difference between the casting and the mold decreases, leading to a reduced driving force for heat transfer.

The h–T curve (Fig. 8c) was finally obtained by correlating the T–t curve with the h–t curve through temporal synchronization.

Reliability and applicability discussion of the IHTC results

The temperature data for each node of the mold was calculated through implicit iteration. Since the temperature data at node 2 is directly related to the inversely calculated interface temperature, the calculated data for this node was compared with the measured temperature data, and their difference is plotted in Fig. 9.

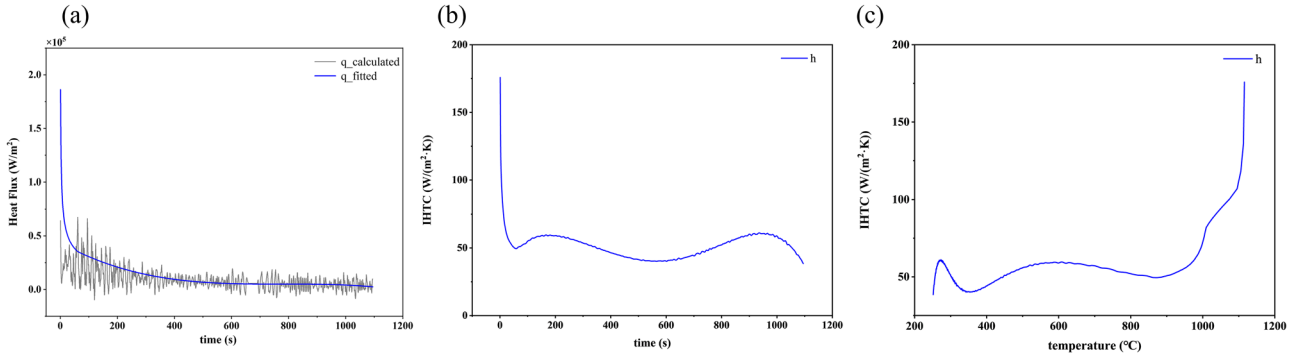

Fig. 8 | Results of the inverse calculation for the heat flux and the IHTC. a Heat flux obtained from the inverse calculation, raw inverse q results (gray curve), fitted q curve (blue line); **b** IHTC vs time; **c** IHTC vs $T_{casting}$.

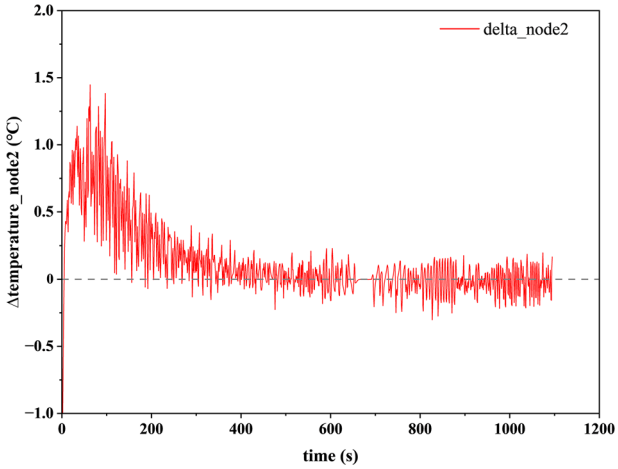

Fig. 9 | Analysis of the convergence of the temperature calculated at node 2.

The calculation error exhibits significant fluctuations during the initial stage (0–200 s), with a maximum error of 1.5 °C. Afterwards, the error quickly approaches 0 °C and remains stable, fluctuating slightly above and below 0 °C with a maximum difference of no more than 0.25 °C. Based on these results, it is concluded that the calculation has successfully converged, and the calculated interfacial temperature and heat flux are reliable and accurate.

The IHTC is primarily influenced by the material and geometric properties of the casting, the material and geometric properties of the clay mold, and the casting process. The composition and size of the bronze were set to match those of ancient Chinese bronze. The thermal parameters of the clay mold were derived from the measured data presented in Table 1. The clay mold used in the temperature measurements was made from native soil sourced from the casting foundry. The casting process, including the pouring time and temperature, was based on ancient casting methods as documented in relevant literature[24]. By taking into account all these factors, accurate data on the IHTC between the clay mold and the casting was obtained under conditions closely resembling those of ancient casting practices.

The IHTC values obtained in this study are based on casting experiments using a specific Western Zhou period clay mold and a typical tin bronze alloy. While variations in either the alloy composition or mold material may alter the interfacial heat transfer behavior, the present methodology offers a robust reference for recalculating the IHTC values applicable to the corresponding conditions. More importantly, compared with conventional approaches that assign a constant IHTC throughout the casting process[30], the IHTC derived in this study effectively integrates the combined effects of contact conduction, interfacial gap convection, and thermal radiation between the mold and the casting. This makes it a more realistic representation of the heat transfer behavior in ancient Chinese bronze casting using clay molds.

Notably, ancient high-quality bronze vessels typically show limited compositional variation and generally fall within the tin bronze system. Moreover, given that successful casting requires the mold's thermal response to fall within a relatively narrow range to accommodate such alloys, the IHTC values obtained here may possess a certain degree of general applicability.

Discussion

This study determined, experimentally, for the first time the IHTC between ancient clay molds and castings by analyzing ancient mold materials. The steps undertaken in this study include: (i) conducting a heat transfer analysis of the casting process of ancient Chinese bronzes using the FDM; (ii) establishing a one-dimensional unsteady heat transfer model; and, (iii) designing a flat-plate casting temperature measurement setup to determine the temperature field of the clay mold and the alloy. In this way, it was possible to obtain the IHTC between castings and clay molds, which has important practical significance.

This study not only addresses the lack of quantitative research on the functional properties of ancient clay molds but also provides a method based on numerical simulations to model the bronze solidification process. This advancement enhances the study of ancient metal artefacts by combining data-driven calculations and precise solutions to address process-related challenges, to take research in this field to a new depth. Observations and computations conducted in this research not only provide a valuable methodological reference for addressing challenges in ancient Chinese casting processes, but also offer critical insights to accurately understand ancient Chinese metalworking techniques.

Zhouyuan, the ancestral homeland of the Zhou people, is characterized by its unique loess resources, which significantly influenced its metallurgical development. As the cradle of Western Zhou culture, this region witnessed the emergence of systematic bronze production by artisans from the pre-Western Zhou period on. During the past century, archaeological excavations have uncovered numerous bronze ritual vessels, establishing Zhouyuan as a major center for bronze casting. Research on key parameters of clay molds unearthed at Zhouyuan holds significance for reconstructing ancient Chinese casting techniques. Building on the thermophysical parameters of the Zhouyuan Western Zhou clay molds, further research will incorporate key boundary conditions into numerical simulations of bronze casting pouring/solidification processes while systematically deriving IHTCs from other major foundry sites (including Shang Dynasty Yinxu and Eastern Zhou Houma bronze-casting complexes). These data will enable comparative analyses of the technological practices and operational principles of artisans across various temporal and spatial contexts.

Scholarship to date has not adequately explored the relationship between the loess distribution and strategic development in Bronze Age

China. While researchers, such as Chang, have argued that Shang and Zhou capital relocations were driven by the need to be near copper sources[31], archaeological evidence challenges this speculation. Major copper deposits are concentrated in the Yangtze River basin, yet no Shang or Zhou capitals were established there. This disconnect highlights the importance of loess in determining the locations of capital cities. While copper could be transported over long distances, the vast quantities of loess required for foundry operations necessitated local sourcing due to logistical considerations. This study, through quantitative research on the casting performance of loess-based clay molds for bronze casting – particularly the establishment of research methodologies for interfacial heat transfer coefficients and the acquisition of key data on Western Zhou mold fragments – provides essential methodological approaches and data resources for deepening understanding of ancient Chinese metallurgical techniques, dynastic resource allocation, geopolitical strategies, and other significant aspects.

Data availability

All data supporting the findings of this study are available within the paper and its Supplementary Information.

Received: 13 November 2025; Accepted: 10 January 2026;
Published online: 21 January 2026

References

1. Gettens, R. J. *The Freer Chinese Bronzes*, Vol. II. 110 (Smithsonian Institute, 1969).
2. Li, Y., Shi, W., Aydin, A., Beroya-Eitner, M. A. & Gao, G. Loess genesis and worldwide distribution. *Earth Sci. Rev.* **201**, 102947 (2020).
3. Yang, H. A brief history of lost-wax casting studies in China's Bronze Age. *Chin. J. Hist. Sci. Technol.* **42**, 136–149 (2021). (In Chinese).
4. Lian, H. P. Analytical study on Warring States period clay molds from Yanxiadu, Yixian County, Hebei Province. *Sci. Conserv. Archaeol.* **4**, 25–31 (1992). (In Chinese).
5. Lian, H. P., Ding, Z. M. & Zhou, X. Analysis of clay molds for metal-mold casting of coins in the Han Dynasty. *Sci. Conserv. Archaeol*. **24**, 87–97 (2012). (In Chinese).
6. Tan, D. R., Xu, H. K. & Huang, L. Research on clay mold casting technology in China's Bronze Age. *Acta Archaeol. Sin.* **2**, 211–250 (1999). (In Chinese).
7. Liu, Y., Song, J. N. & Liu, X. Y. Analytical testing of bronze casting remains unearthed from Zhouyuan. *Archaeol. Cultural Relics.* **4**, 94–100 (2007). (In Chinese).
8. Tian, J. H. Preliminary study on several clay molds unearthed in Henan Province. In *Proc. 5th Annual Conference of China Association for Preservation Technology of Cultural Relics.* Nanjing Museum, 296–301 (2007). (In Chinese).
9. Zhao, G. Y. & Guo, J. F. Composition and structure of clay mold materials for Yinxu bronze vessels. *J. Anyang Inst. Technol.* **6**, 34–38 (2009). (In Chinese).
10. Zhao, G. Y. et al. Effect of composition on the properties of Shang-Zhou bronze vessel clay molds. *J. Anyang Inst. Technol.* **9**, 23–26 (2010). (In Chinese).
11. Dantzig, J. A. & Rappaz, M. *Solidification*, 6 (Science Press, 2015). (In Chinese)
12. Guthrie, R. et al. Measurements, simulations, and analyses of instantaneous heat fluxes from solidifying steels to the surfaces of twin roll casters and of aluminum to plasma-coated metal substrates. *Metall. Mater. Trans. B.* **31**, 1031–1047 (2000).
13. Griffiths, W. A model of the interfacial heat-transfer coefficient during unidirectional solidification of an aluminum alloy. *Metall. Mater. Trans. B.* **31**, 285–295 (2000).
14. Lewis, R. W., Ransing, R. S. & B, M. T. A correlation to describe interfacial heat transfer during solidification simulation and its use in the optimal feeding design of castings. *Metall. Mater. Trans. B.* **29**, 437–448 (1998).
15. Guo, Z. P., Xiong, S. M., Cao, S. X. & Cui, Z. J. Establishment of inverse heat conduction model and its application in solving interfacial heat flux. *Acta Metall. Sin.* **6**, 607–611 (2007). (In Chinese).
16. Shao, H. et al. Measurement of interfacial heat transfer coefficient in aluminum alloy investment precision casting. *Foundry Zhuzao* **63**, 1010–1013+1018 (2014). (In Chinese).
17. Tao, W. Q. *Heat Transfer*, 5th edn., 37 (Higher Education Press, 2019). (In Chinese)
18. Huang, C. H., Yuan, I. C. & Ay, H. A three-dimensional inverse problem in imaging the local heat transfer coefficients for plate finned-tube, heat exchangers. *Int. J. Heat. Mass Transf.* **46**, 3629–3638 (2003).
19. Bazhenov, V. et al. Investigation of the interfacial heat transfer coefficient at the metal–mold interface during casting of an A356 aluminum alloy and AZ81 magnesium alloy into steel and graphite molds. *Int. J. Metalcasting* **15**, 625–637 (2021).
20. Sun, Z., Hu, H. & Niu, X. Determination of heat transfer coefficients by extrapolation and numerical inverse methods in squeeze casting of magnesium alloy AM60. *J. Mater. Process. Technol.* **211**, 1432–1440 (2011).
21. Chen, L., Wang, Y., Peng, L., Fu, P. & Jiang, H. Study on the interfacial heat transfer coefficient between AZ91D magnesium alloy and silica sand. *Exp. Exp. Therm. Fluid Sci.* **54**, 196–203 (2014).
22. Elkins, B. S. *Challenges for the Accurate Determination of the Surface Thermal Condition via In-Depth Sensor Data*. PhD thesis (University of Tennessee, 2011).
23. Huang, Q., Yue, L., Li, X. & Wang, P. A correlation to calculate time constant of thermocouples. *Appl. Therm. Eng.* **246**, 122920 (2024).
24. Jaremkiewicz, M., Taler, D. & Sobota, T. Measuring transient temperature of the medium in power engineering machines and installations. *Appl. Therm. Eng.* **29**, 3374–3379 (2009).
25. Hua, J. M. *Ancient Chinese Metal Technology: A Civilization Forged by Copper and Iron*, 120–127 (Elephant Press, 1999). (In Chinese)
26. Zhao, K. M., Ren, D. X., Wang, B. & Chang, Y. Investigation of the interfacial heat transfer coefficient of sheet aluminum alloy 5083 in warm stamping process. *Int. J. Heat. Mass Transf.* **132**, 293–300 (2019).
27. Zhang, W. et al. Inverse calculation of interfacial heat transfer coefficient during solidification of circular cast steel castings by no-bake furanresin bounded sand casting. *Int. J. Metalcasting* **17**, 2128–2137 (2023).
28. Beck, J. V. *Inverse Heat Conduction: Ill-Posed Problems*, 145 (Wiley-Interscience, 1985).
29. Oliveira, A. V. S., Avrit, A. & Gradeck, M. Thermocouple response time estimation and temperature signal correction for an accurate heat flux calculation in inverse heat conduction problems. *J. Heat. Mass Transf.* **185**, 122398 (2022).
30. Pola, A., Mödlinger, M., Piccardo, P. & Montesano, L. Casting simulation of an Austrian Bronze Age sword hilt. *Jom* **67**, 1637–1645 (2015).
31. Chang, K. C. *Zhongguo Qingtong Shidai [The Bronze Age of China]*. (Sanlian Bookstore, 2013). (In Chinese)

Acknowledgements

We express our sincere gratitude to Dr. Ding Hong (Shanxi University), and Mr. Jiang Ling for their valuable contributions to this research.

Author contributions

Huan Yang: Conceptualization, Methodology, Investigation, Writing - Original Draft; Minghui Fang: Methodology, Software, Formal analysis, Writing - Review & Editing; Jiangning Song: Archaeological background, Data; Tonia Eckfeld: Writing - Review & Editing; Junchang Yang: Supervision.

Competing interests
The authors declare no competing interests.

Additional information
Supplementary information The online version contains supplementary material available at https://doi.org/10.1038/s40494-026-02318-9.

Correspondence and requests for materials should be addressed to Huan Yang.